Flow of Magnetized Casson Hybrid Nanofluid with Nonlinear Thermal Radiation and Modified Heat Flux Model

Akhtar Ali[a], Manzoor Ishaq[a] , Sami Ullah Khan[b*],

[a] *Department of Mathematics, Government College University, Faisalabad and 38000, Pakistan*

[b,*] *Department of Mathematics, Namal University, Mianwali and 42250,Pakistan*[*]

[*] *Corresponding author; E-mail: sk_iiu@yahoo.com*

Abstract:

This study aims to present the thermal aspects of magnetized hybrid nanofluid in the presence of viscous dissipation and nonlinear radiated effects. Thermal behavior of hybridized nanofluid is integrated by the addition of copper (Cu) *and silver* (Ag) *nanomaterials in ethyl glycol* $(C_6H_{12}O_6)$ *base fluid. The heat transfer analysis is inspected with enrollment of nonlinear radiated effects. Both energy and mass transfer expressions are extended by using the updated Cattaneo-Christov modelling. The problem is solved numerically using the shooting method. Comparative findings are simulated for hybrid nanofluid* $(Cu-Ag/C_6H_{12}O_6)$ *and mono nanofluid* $(Cu/C_6H_{12}O_6)$*. It is observed change in Casson fluid parameter leads to enhancement of velocity profile. The heat transfer enhances due to nanoparticles volume fraction and temperature ratio parameter. Moreover, the concentration profile declines due to* thermal concentration number and Schmidt number.

Keywords: *Casson fluid, hybrid nanofluid, viscous effects, shooting method, nonlinear radiation, Convective boundary conditions.*

1. INTRODUCTION

Many researchers and industrialists are attracted towards nanofluids due to highly recommendable characteristics of heat transfer and energy efficiency across various systems. The thermal properties of traditional fluids such as water, oil and ethyl-glycol are low, offering minimum thermal features. These properties can be improved dramatically by adding nanomaterials to base fluids. The advantages of nanofluids in industries include enhanced design capabilities, faster, and improved energy efficiency in various systems, all at a very low cost. Due to extraordinary enhanced thermal properties, nanofluids are used in various sectors, including electronics, automotive engines, and renewable energy devices. Nanofluids play a vital role in developing the nanotechnology, material sciences and energy sectors. The sustainability and versatility of nanofluids are considered to enhance energy utilization and minimize waste. The appropriate choice of nanomaterial and size of nanoparticles rectifies the heat transfer rate. Further, the sustainability and compatibility of nanomaterials is more effective. Ali et al. (2021) studied the advancement in heat transfer with utilization of carbon based nanomaterial. Li et al. (2021) explained thermal significance and impreesive heat transfer influence due to nanofluid flow. Pavía et al. (2021) investigated thermal outcomes of graphite nanomaterials and inspected heat transfer enhancement. Sheikholeslami et al. (2021) syncretized the improvement in heat transfer due to nanofluid, preserving significance to solar collectors and photovoltaic cells. Sharma et al. (2022) illustrated the recent advancements renewable energy by studying nanofluid properties. The importance of nanofluid in oil recovery processes was focused by Khoramian et al. (2022). The hydro-thermal behavior of nanofluid underlying radiated effects was predicted by Acharya et al. (2022). A critical review on sustainability and synthesis approaches of nanofluids was accounted by Wang et al. (2023). Bhatti et al. (2023) portrayed the vital characteristic of nanofluids by using various types of nanoparticles. The comprehensive insights of heat transmission process by utilizing non-Newtonian nanofluids were discussed by Nabwey et al.

(2023). Ahmed et al. (2024) performed the numerical treatment on magnetized Maxwell nanofluid nonlinear radiated effects and activated energy. The thermo-physical behavior of nanofluid (Al_2O_3/ H_2O) was visualized by Bani-Fwaz et al. (2024). Rahman et al. (2024) focused development methods and essential characteristics of nanofluid. Thermal performance and optimal concentration of different nanofluids were examined by Alkasmoul et al. (2025). The contributions of nanoparticles under the thermal radiation phenomenon were highlighted by Iqbal et al. (2025).

Hybrid nanofluids (HNF) are colloidal suspensions of two or more types of nanomaterials in a base fluid. The hybrid nanofluid (HNF) proposed advancement in heat transfer process due to improved thermal characteristics makes it superior to nanofluids. Many researchers focused on thermos-physical characteristics. The significance of hybrid nanofluids has been estimated as backbone of various sectors across renewable energy and geothermal systems. In industrial sectors, the HNF are widely useable in cooling processes for electronic devices and data centers. The HNF are considered as a cooling agent for engine and fuel efficiency in automotive engineering. In heat exchangers, the applications of HNF enhances the energy efficiency and reduced the operational cost. Muneeshwaran et al. (2021) studied the involvement of HNF in heat transfer enhancement. The heat transfer analysis due to HNF with velocity slip boundary constraints were explored by Kumar et al. (2021). Dero et al. (2022) predicted the stability analysis of magnetized hybrid nanofluid along with suction/injection impact. Waqas et al. (2022) performed a comparative modelling of HNF and MNF in elastic surface radiated flow. Hayat et al. (2023) investigated the analysis of heat transfer and entropy generation for squeezed flow of HNF against utilizing Cattaneo-Christov (CC) model. Mishra et al. (2023) investigated the heat and mass transfer performance against the HNF, consisting of copper and aluminum nanoparticles immersed in water base fluid. Thermal analysis of hybrid nanofluid by using convective boundary constraints has been observed by Algehyne et al. (2024). The entropy analysis of magnetized HNF in a porous media were responded by Oudina et al. (2024). Ishaq et al. (2025) detected thermal stability of Casson HNF with radiation effects. Khan et al. (2025) accounted the thermal enhancement due to HNF with chemical sepcies and implementation of CC model.

Casson fluids are classified as a non-Newtonian fluid exhibits both characteristics the novel shear thinning and thickening consequences. The extensive application of Casson material are observed in human blood, printing ink, and chocolate. The innovative rheological characteristics of Casson fluid model offer wide range of applications across various sectors including biomedical engineering, polymer processing and food industry. Khan et al. (2022) simulated the heat and mass transfer analysis by using Casson fluid model. The stratified flow of Casson fluid with microorganisms over a stretching sheet were examined by Lone et al. (2023). Moatimid et al. (2024) rectified the nonlinear instability characteristics of electrified Casson fluids via analytically approach. Double-diffusive mixed convection of Casson fluid were elaborated by Bathmanaban et al. (2024). A triple diffusive modeling of Casson fluid with slip effects were proposed by Faridi et al. (2025).

1.1. Proposed model

It has been observed that several investigations are performed for enhancement of heat transfer due to Casson hybrid nanofluid by considering various thermal features. However, the investigation of thermal profile due to magnetized hybrid nanofluid $\left(Cu - Ag / C_6H_{12}O_6\right)$ with applications of viscous dissipation and nonlinear radiated effects has not been properly focused. This study aims to present mathematical modeling Casson hybrid nanofluid with implementation of non-Fourier approach. The convective thermal conditions are imposed to analyze the heat transfer impact. After simplifying the problem into dimensionless form, shooting technique is used with effective accuracy. Comparative findings are proposed for mono nanofluid and hybrid nanofluid. The novelty of current model lies in comprehensive inspection of mass and heat transfer dynamics in Casson HNF, composed of silver and copper nanoparticles with ethylene glycol base liquid. The integration of HNF effectively boosted thermal features of base materials as compared to mono nanofluid. The implementation of advanced Fourier's model accounts the finite proportion features which cannot be assessed by using the classical Fourier's model. Moreover, consideration of nonlinear radiated features, presenting novel importance in high-temperature systems. The proposed model offers understanding of advanced thermal transport dynamics and applications to solar energy systems, high temperature thermal systems, nuclear technologies and automobile thermal management.

1.2. Research questions

- How does the Casson fluid parameter impact the thermal and momentum profiles for hybrid and mono nanofluids?
- What is the role of nonlinear radiated phenomenon in enhancing the thermal behavior of HNF suspension?
- How does the non-Fourier thermal flux influence the finite thermal distribution and finite propagation framework as compared to traditional Fourier's heat conduction?
- How does the HNF suspension improve the thermal performance of the nanofluid compared with traditional fluids under convective boundary conditions?"

2. Mathematical formulation

2.1. Flow assumptions and governing equations

Consider an incompressible, steady, and two-dimensional flow of magnetized Casson hybrid nanofluid associated with a porous stretchable sheet. The velocity components in horizontal and normal to the configuration are responded via u and v, respectively. Let $u = cx$ be velocity of fluid indorsed by stretched surface. The magnetic field is entertained normal to the sheet. The thermal relaxation analysis effects are examined by the implementation of Cattaneo-Christov (CC) model. Further, nonlinear radiative features and viscous dissipative relations are used in energy equations. The surface temperature, wall temperature and ambient temperature of hybrid nanofluid are escalated through T, T_w and T_∞. The modelled equations under such assumptions are (Ishaq et al., 2025).

$$\frac{\partial u}{\partial x}+\frac{\partial v}{\partial y}=0, \tag{1}$$

$$u\frac{\partial u}{\partial x}+v\frac{\partial u}{\partial y}=\nu_{hnf}\left(1+\frac{1}{\beta^*}\right)\frac{\partial^2 u}{\partial y^2}-\nu_{hnf}\frac{u}{k}-\frac{\sigma_{hnf}B_0^{\,2}}{\rho_{hnf}}u, \tag{2}$$

$$u\frac{\partial T}{\partial x}+v\frac{\partial T}{\partial y}+\lambda_1\begin{bmatrix} u\dfrac{\partial u}{\partial x}\dfrac{\partial T}{\partial x}+v\dfrac{\partial v}{\partial y}\dfrac{\partial T}{\partial y} \\ +u\dfrac{\partial v}{\partial x}\dfrac{\partial T}{\partial y}+2uv\dfrac{\partial^2 T}{\partial x\partial y} \\ +v\dfrac{\partial u}{\partial y}\dfrac{\partial T}{\partial x}+v^2\dfrac{\partial^2 T}{\partial y^2} \\ +u^2\dfrac{\partial^2 T}{\partial x^2}\end{bmatrix}=\begin{bmatrix}\dfrac{K_{hnf}}{\left(\rho C_p\right)_{hnf}}\dfrac{\partial^2 T}{\partial y^2}+\dfrac{\mu_{hnf}}{\left(\rho C_p\right)_{hnf}}\left(1+\dfrac{1}{\beta^*}\right)\left(\dfrac{\partial u}{\partial y}\right)^2 \\ +\dfrac{16\sigma^*}{3\left(\rho C_p\right)_{hnf}k^*}\dfrac{\partial}{\partial y}\left(T^3\dfrac{\partial T}{\partial y}\right)\end{bmatrix}, \tag{3}$$

$$u\frac{\partial C}{\partial x}+v\frac{\partial C}{\partial y}+\lambda_2\begin{bmatrix} u^2\dfrac{\partial^2 C}{\partial x^2}+v^2\dfrac{\partial^2 C}{\partial y^2}+2uv\dfrac{\partial^2 C}{\partial x\partial y} \\ +v\dfrac{\partial u}{\partial y}\dfrac{\partial C}{\partial x}+u\dfrac{\partial v}{\partial x}\dfrac{\partial C}{\partial y}+v\dfrac{\partial v}{\partial y}\dfrac{\partial C}{\partial y} \\ +u\dfrac{\partial u}{\partial x}\dfrac{\partial C}{\partial x}\end{bmatrix}=D_B\frac{\partial^2 C}{\partial y^2}-k_r^{\,2}\left(C-C_\infty\right) \tag{4}$$

with ρ_{hnf} (density), μ_{hnf} (dynamic viscosity), B_0 (magnetic field intensity), σ_{hnf} (Stefan Boltzmann constant), K_{hnf} (thermal conductivity of hybrid nanofluid), $\left(\rho C_p\right)_{hnf}$ (specific heat

capacity of hybrid nanofluid), D_B (Brownian motion diffusivity), β^* (Casson constant) k_r (chemical reactivity), λ_1 (thermal relaxation), λ_2 (concentration relaxation).

The boundary conditions are (Ishaq et al. (2025)):

$$\left.\begin{aligned} &u = u_w = cx,\ v = -v_w,\ -K_{hnf}\left(\frac{\partial T}{\partial y}\right) = h_f\left(T_f - T\right), C = C_w \ at\ y = 0, \\ &u \to 0, \frac{\partial u}{\partial y} \to 0, T \to T_\infty C \to C_\infty,\ y \to \infty. \end{aligned}\right\} \tag{5}$$

where h_f be the heat transfer coefficient. It has been remarked that above boundary constraints are related to moving surfaces flow. The heat and mass transfer analysis due to such moving configurations attributes various applications in manufacturing phenomenon, coating procedures, polymer extrusion, processing engineering and drag reduction industries.

2.2. Similarity variables

Dimensionless variables are defined as (Ishaq et al. (2025)):

$$v = -\sqrt{\nu_f c} f, \zeta = \sqrt{\frac{c}{\nu_f}} y,\ u = cxf',\ \theta = \frac{T - T_\infty}{T_w - T_\infty}, \phi = \frac{C - C_\infty}{C_w - C_\infty}. \tag{6}$$

Subject to following dimensionless equations:

$$S_1\left(1 + \frac{1}{\beta^*}\right) f''' - \left(S_1\beta + S_3\beta_1\right) f' - S_2\left(f'^2 - ff''\right) = 0, \tag{7}$$

$$\begin{aligned} &\left(S_4 + R\left[\left(\theta_w - 1\right)\theta + 1\right]^3\right)\theta'' + 3R\left[\left(\left(\theta_w - 1\right)\theta + 1\right)^2\left(\theta_w - 1\right)\theta'^2\right] + \\ &\Pr\left[S_5\left(f\theta' - \delta_T\left(ff'\theta' + f^2\theta''\right)\right) + S_1\left(1 + \frac{1}{\beta^*}\right)Ecf''^2\right] = 0, \end{aligned} \tag{8}$$

$$\phi'' - Sc\left(\beta_4\phi - f\phi'\right) - \beta_3\left(ff'\phi' + f^2\phi''\right) = 0. \tag{9}$$

with

$$\left.\begin{aligned} &f(0) = S, f'(0) = 1,\ A_4\theta'(0) = -Bi\left[1 - \theta(0)\right], \phi(0) = 1 \ at\ \zeta = 0, \\ &f'(\infty) \to 0,\ \theta'(\infty) \to 0, \phi(\infty) \to 0 \ at\ \zeta \to \infty. \end{aligned}\right\} \tag{10}$$

where $Ec = U_w^{\,2} / (C_p)_f (T_w - T_\infty)$ be Eckert number, $\beta_1 = \sigma_f B_o^{\,2} / \mathrm{c}\,\rho_f$ denotes the Hartmann parameter, $\beta = \upsilon_f / \mathrm{c}\,k$ represents porosity parameter, $\Pr = \nu_f \left(\rho C_p\right)_f / k_f$ combines Prandtl number, $R = 16\sigma^* T_\infty^{\,3} / 3k^* k_f$ shows thermal radiation number, $Sc = \nu_f / D_B$ is the Schmidt number, $\theta_w = T_w / T_\infty$ be temperature ratio number. $\delta_T = \lambda_1 c$ illustrates thermal relaxation parameter, $\beta_3 = \lambda_2 c$ demonstrates relaxation concentration parameter, $\beta_4 = Kr^2 / \mathrm{c}$ demonstrates chemical reactive number, $Bi = \frac{h_f}{k_f}\sqrt{\frac{\nu_f}{b}}$ be Biot parameter.

The thermal constants are:

$$S_1=\frac{\mu_{hnf}}{\mu_{nf}},S_2=\frac{\rho_{hnf}}{\rho_{nf}},\ S_3=\frac{\sigma_{hnf}}{\sigma_{nf}},S_4=\frac{K_{hnf}}{K_{nf}},S_5=\frac{(\rho C_p)_{hnf}}{(\rho C_p)_{nf}}.$$

2.3. Thermophysical properties of hybrid nanofluid

Table 1 captures the thermophysical properties of nanoparticles and base fluid numerically. The mathematical form of the thermal properties of hybrid nanofluid and mono fluid are predicted in Table 2.

Table:1. Physical properties of copper and silver nanoparticles and ethyl-glycol base fluid.

Physical Properties	Cu (Copper)	Ag (Silver)	Ethylene glycol $(C_6H_{12}O_6)$
$\rho(kgm^{-3})$	8933	10500	1115
$C_p(Jkg.k)$	385	235	2430
σ	-	6.63×10^7	24.4
$\kappa(W.(m.k))$	401	429	0.253

Table 2: Mathematical relations for nanofluid and hybrid nanofluid.

Characteristics	Nanofluid and Hybrid Nanofluid
Density	$\rho_{nf}=(1-\phi)\rho_f+\phi\rho_s$ $\rho_{hnf}=(1-\phi_2)\left[(1-\phi_1)\rho_f+\phi_1\rho_{s1}\right]+\phi_2\rho_{s2}$
Heat capacity	$(\rho C_p)_{nf}=\left[(1-\phi)(\rho C_p)_f+\phi(\rho C_p)_s\right]$ $(\rho C_p)_{nf}=(1-\phi_2)\left[(1-\phi_1)(\rho C_p)_f+\phi_1(\rho C_p)_{s1}\right]+\phi_2(\rho C_p)_{s2}$
Dynamic viscosity	$\mu_{nf}=\frac{\mu_f}{(1-\phi)^{2.5}}$ $\mu_{nf}=\frac{\mu_f}{(1-\phi_1)^{2.5}(1-\phi_2)^{2.5}}$
Thermal conductivity	$k_{nf}=\frac{k_s+(n-1)k_f-(n-1)\phi(k_f-k_s)}{k_s+(n-1)k_f+(n-1)\phi(k_f-k_s)}*k_f\ \ Where\ n=3/\psi$ $k_{hnf}=\frac{k_{s1}+(n-1)k_f-(n-1)\phi_1(k_f-k_{s1})}{k_{s1}+(n-1)k_f+\phi_1(k_f-k_{s1})}*k_f$ $k_{hnf}=\frac{k_{s2}+(n-1)k_{bf}-(n-1)\phi_2(k_{bf}-k_{s2})}{k_{s2}+(n-1)k_{bf}+\phi_2(k_{bf}-k_{s2})}*k_f$

2.4. Engineering flow quantities

Skin friction coefficient $Cf_x\left(\mathrm{Re}_x\right)^{1/2}$, Nusselt number $Nu_x\left(\mathrm{Re}_x\right)^{-1/2}$ and Sherwood number $Sh_x\left(\mathrm{Re}_x\right)^{-1/2}$ are:

$$\left.\begin{aligned} &C_{fx}=\frac{\tau_w}{\rho u_w^2}, Nu_x=\frac{xq_w}{k_f\left(T_w-T_\infty\right)}, Sh_x=\frac{xJ_w}{D_B\left(C_w-C_\infty\right)}\\ &\tau_w=\mu_{hnf}\left[\left(\frac{\partial u}{\partial y}\right)\right]_{y=0},\ q_w=-\left(k_{hnf}+\frac{16T_\infty^3\sigma^*}{3k^*}\right)\left(\frac{\partial T}{\partial y}\right)_{y=0}, J_w=-D_B\left(\frac{\partial C}{\partial y}\right)_{y=0}. \end{aligned}\right\} \tag{11}$$

$$\left.\begin{aligned} &\mathrm{Re}_x^{1/2}\,C_{fx}S_1=S_2f''(0),\\ &\mathrm{Re}_x^{-1/2}\,Nu_x=-\left(S_4+R\left[1+(\theta_w-1)\theta(0)\right]^3\right)\theta'(0),\\ &Sh_x\left(\mathrm{Re}_x\right)^{-1/2}=-\phi'(0). \end{aligned}\right\} \tag{12}$$

3. Methodology

This section deals with implementation of shooting technique for solving the problem. Owing to higher accuracy and less residual error, the choice of shooting technique is preferred. This scheme is effective for computation of many complex problems involving nonlinear and multi-dimensional equations. Shooting technique convert the higher order system into first order relations with the help of appropriate substitutions. Furthermore, shooting technique does not consist of discretization steps, like other numerical schemes. Defining new variables:

$$\left.\begin{aligned} &f=\gamma_1, f'=\gamma_2, f''=\gamma_3, f'''=\gamma_3',\\ &\theta=\gamma_4, \theta'=\gamma_5, \theta''=\gamma_5',\\ &\phi=\gamma_6, \phi'=\gamma_7, \phi''=\gamma_7'. \end{aligned}\right\} \tag{13}$$

Yielding:

$$\gamma_3'=\frac{1}{S_1\left(1+\frac{1}{\beta^*}\right)}\left[\left(S_1\beta+S_3\beta_1\right)\gamma_2+S_2\left(\gamma_2^{\,2}-\gamma_1\gamma_3\right)\right], \tag{14}$$

$$\gamma_5'=\frac{-3R\left[\left(\gamma_4(\theta_w-1)+1\right)^2(\theta_w-1)\gamma_5^{\,2}\right]-\mathrm{Pr}\left[S_5\left(\gamma_1\gamma_5-\delta_T\gamma_1\gamma_2\gamma_5\right)+S_1\left(1+\frac{1}{\beta^*}\right)Ec\gamma_3^{\,2}\right]}{\left[\left(S_4+R\left(\gamma_4(\theta_w-1)+1\right)^3\right)-\mathrm{Pr}\,\delta_T\gamma_1^{\,2}S_5\right]} \tag{15}$$

$$\gamma_7'=\frac{\left[Sc\left(\beta_4\gamma_6-\gamma_1\gamma_7\right)+\beta_3\gamma_1\gamma_2\gamma_7\right]}{\left(1-\beta_3\gamma_1^{\,2}\right)}. \tag{16}$$

with:

$$\left.\begin{aligned} &\gamma_1(0)=S, \gamma_2(0)=1, S_4\gamma_5'(0)=-Bi\left[1-\gamma_4(0)\right], \gamma_6(0)=1, at\ \zeta=0,\\ &\gamma_2(\infty)\to 0, \gamma_5(\infty)\to 0, \gamma_6(\infty)\to 0\ at\ \zeta\to\infty. \end{aligned}\right\} \tag{17}$$

The suitable selection of grid point and error estimation justify the convincing efficiency of this scheme. A step size of $\Delta\zeta=0.02$ is followed to perform the simulations. The accuracy of solution is considered to be 10^{-4}. The representation of numerical steps is presented with help of Fig. 1.

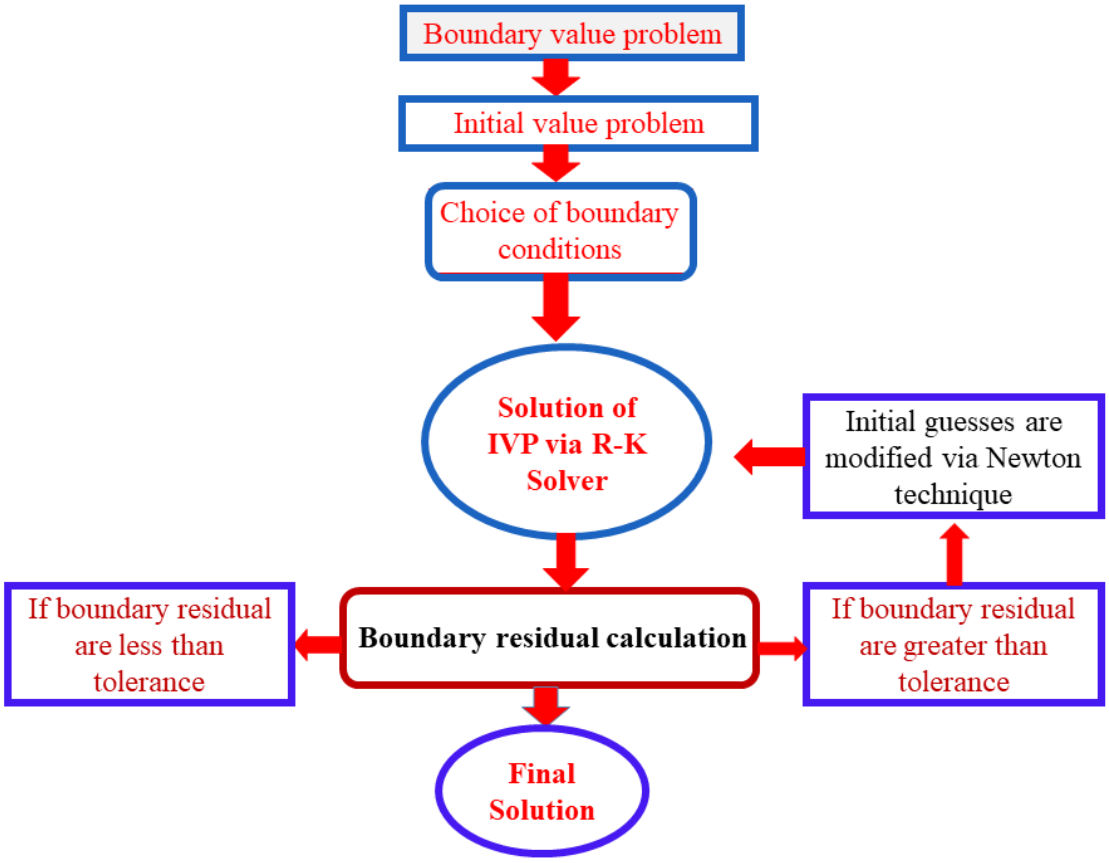

Fig. 1. Numerical chart for shooting scheme.

4. Validation of results

The validation of numerical results is based on comparison of solution with results of Hayat et al. (2010) in table 3 under limiting case. A convincing accuracy of results have been examined.

Table 3: Validation of results with Hayat et al. (2010).

β_1	Hayat et al. (2010)	Present results
0	-1.000000	-1.000000
0.5	-1.224747	-1.224745
1.5	-1.581147	-1.581148
2.0	-1.732057	-1.732055

5. Result and discussion

Physical insight of parameters influences the fluid velocity (f'), temperature (θ) and concentration (ϕ) profiles is visualized in this section. Comparative thermal findings are proposed for hybrid nanofluid and mono nanofluid for multiple parameters like Hartmann number (β_1), Casson fluid coefficient (β), porosity parameter (α), Suction parameter (S), Temperature ratio

parameter (θ_w), Biot number (Bi), Radiation number (R), Eckert number (Ec), Chemical reactive number (β_4), thermal relaxation number (δ_T), Prandtl number (Pr), concentration relaxation number (β_3) and Schmidt number (Sc). Fig. 2(a) escalates the physical behavior of Hartmann number β_1 on velocity profile f'. The velocity profile exhibits a declining profile against β_1. The physical relevance of such observations are subject to stronger Lorentz force. The declination in velocity profile is higher for nanofluid. The discussion on f' due to Casson fluid coefficient β in case of mono $(Cu/C_6H_{12}O_6)$ and hybrid $(Cu-Ag/C_6H_{12}O_6)$ nanofluid is predicted via Fig. 2(b). The profile of f' enhances for β. Such observations are physically associated to shear thickening and thinning nature of Casson fluid. In fact, the shear thinning and thickening features of Casson fluid fluctuates the flow thorough boundary surface. Fig. 2(c) illustrates the effect of porosity parameter α on f'. The higher values of α boosted f' for both suspensions. The enlarging values of porosity parameter associated to permeability of porous media which boosted the flow. The impact of suction parameter S on f' is responded in Fig. 2(d). The velocity profile increase due to larger values of S. Fig. 3(a) captures thermal aspects of Prandtl number Pr for temperature profile θ. It can be observed that temperature profile declines for Pr for $(Cu/C_6H_{12}O_6)$ and $(Cu-Ag/C_6H_{12}O_6)$. Physically, higher Pr reduces the thermal diffusivity which leads to decrement on heat transmission. The influence of radiation parameter R on θ is exploited through Fig. 3(b). It can be noticed that θ rises when radiation effects are prominent. Such outcomes physically involve the transmission of energy through electromagnetic waves. In order to observance the variation of due to thermal relaxation parameter , Fig. 3(c) is presented. Change in δ_T reduces θ which is physically associated to finite waves propagation features.

Fig. 3(d) examines the role of Biot number on θ. Temperature boosted due to Bi. Such outcomes are physically associated to direction involvement of Bi with coefficient of thermal relation. Fig. 3© determines results of Eckert number Ec on prediction of θ. The enlarging variation of Ec grows the field of θ. These outcomes physically influences the enhancement of kinetic energy due to Ec. Fig. 3(f) proposed that temperature profile enhances for larger volume fraction ϕ_1. The role of temperature ratio parameter θ_w on θ has been noticed in Fig. 3(g). It noticed that θ increases due to θ_w. Physical aspects for such increasing results is based on increment of thermal energy in convective surface. Fig. 4(a) demonstrates the effective impact of Schmidt number Sc on concentration profile ϕ. Schmidt number reduces the profile of ϕ. Physically, Sc declines the mass diffusivity which turns down the concentration. The impact of thermal concentration number β_3 on ϕ is focused in Fig. 4(b). Change in β_3 decreases the ϕ. Fig. 4(c) encapsulates the results for chemical reactive number β_4 on ϕ. The profile of ϕ declines due to β_4.

Fig. 5(a) elaborates variation of skin friction coefficient $Cf_x\,\mathrm{Re}_x^{1/2}$ against Hartmann number β_1 for numerous values of porosity number α. A lower variation in skin friction is predicted for α. In order to assess the variation of $Cf_x\,\mathrm{Re}_x^{1/2}$ against S by varying β_1, Fig. 5(b) is plotted. A decrement in $Cf_x\,\mathrm{Re}_x^{1/2}$ due to β_1 is observed. Fig. 6(a) presents the results for Nusselt number $\mathrm{Nu}_x\,\mathrm{Re}_x^{-1/2}$ against Bi is noticed by varying Pr. It can be noticed that $\mathrm{Nu}_x\,\mathrm{Re}_x^{-1/2}$ slows down for Pr. Fig. 6(b) syncretizes the variation of Nusselt number $\mathrm{Nu}_x\,\mathrm{Re}_x^{-1/2}$ as function of R by varying Pr. The Nusselt number declines for Pr. Fig. 7(a) elucidates the profile Sherwood number $Sh_x\,\mathrm{Re}_x^{-1/2}$ against β_3 for numerous values of Sc. $Sh_x\,\mathrm{Re}_x^{-1/2}$ profile declines due to Sc. The results for $Sh_x\,\mathrm{Re}_x^{-1/2}$ and Sc due to β_3 are exhibited in Fig. 7(b). Higher β_3 enhances the profile

of $Sh_x \operatorname{Re}_x^{-1/2}$. Table 4 manipulates the numerical outcomes of wall shear force for different parameters. The skin friction reduces for α, β and β_1. The numerical computations for understanding of Nusselt number against flow parameters are captured in table 5. The Nusselt number increases for Ec while change in ϕ_1 and θ_w leads to improvement of Nusselt number. Table 6 represents the numerical outcomes of Sherwood number $Sh_x \operatorname{Re}_x^{-1/2}$ by varying different flow parameters. Higher β_4 and Sc corresponds to enhancement of $Sh_x \operatorname{Re}_x^{-1/2}$.

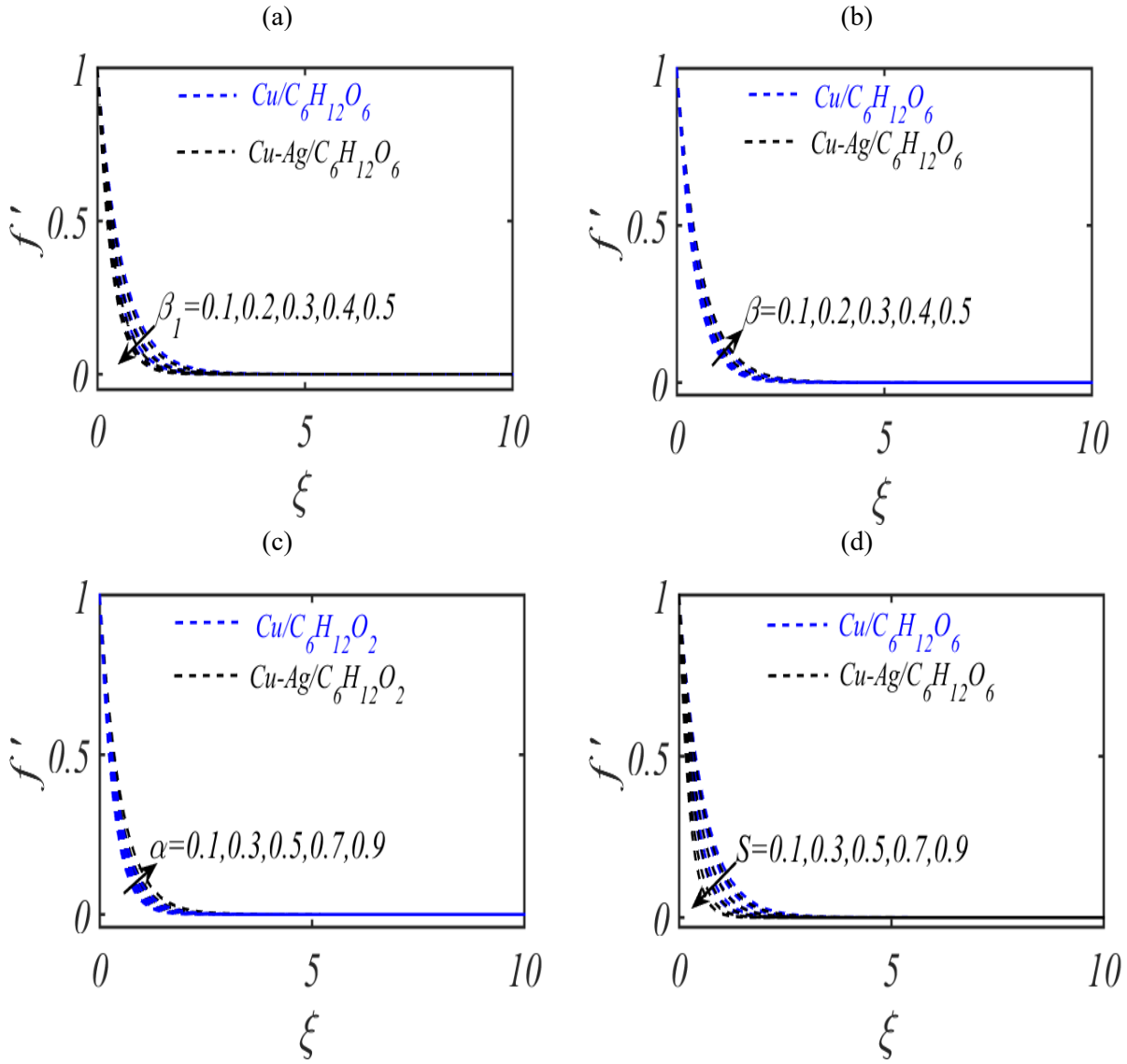

Figure. 2(a-d): The impact of (a) β_1 (b) β (c) α (d) S versus velocity distribution f'.

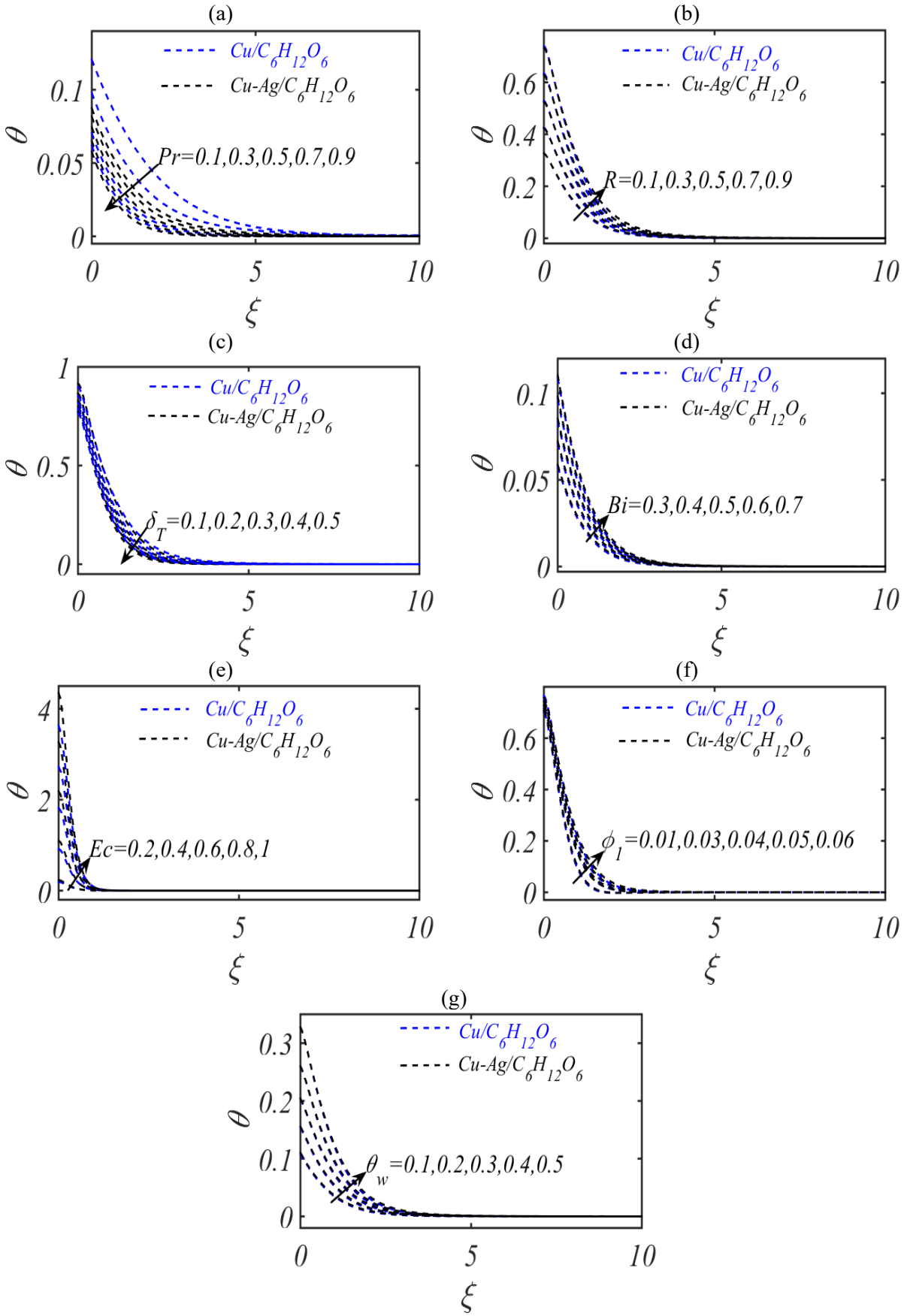

Figure. 3(a-g): The impact of (a) Pr (b) R (c) δ_T (d) Bi (e) Ec (f) ϕ_1 (g) θ_w across the temperature profile θ.

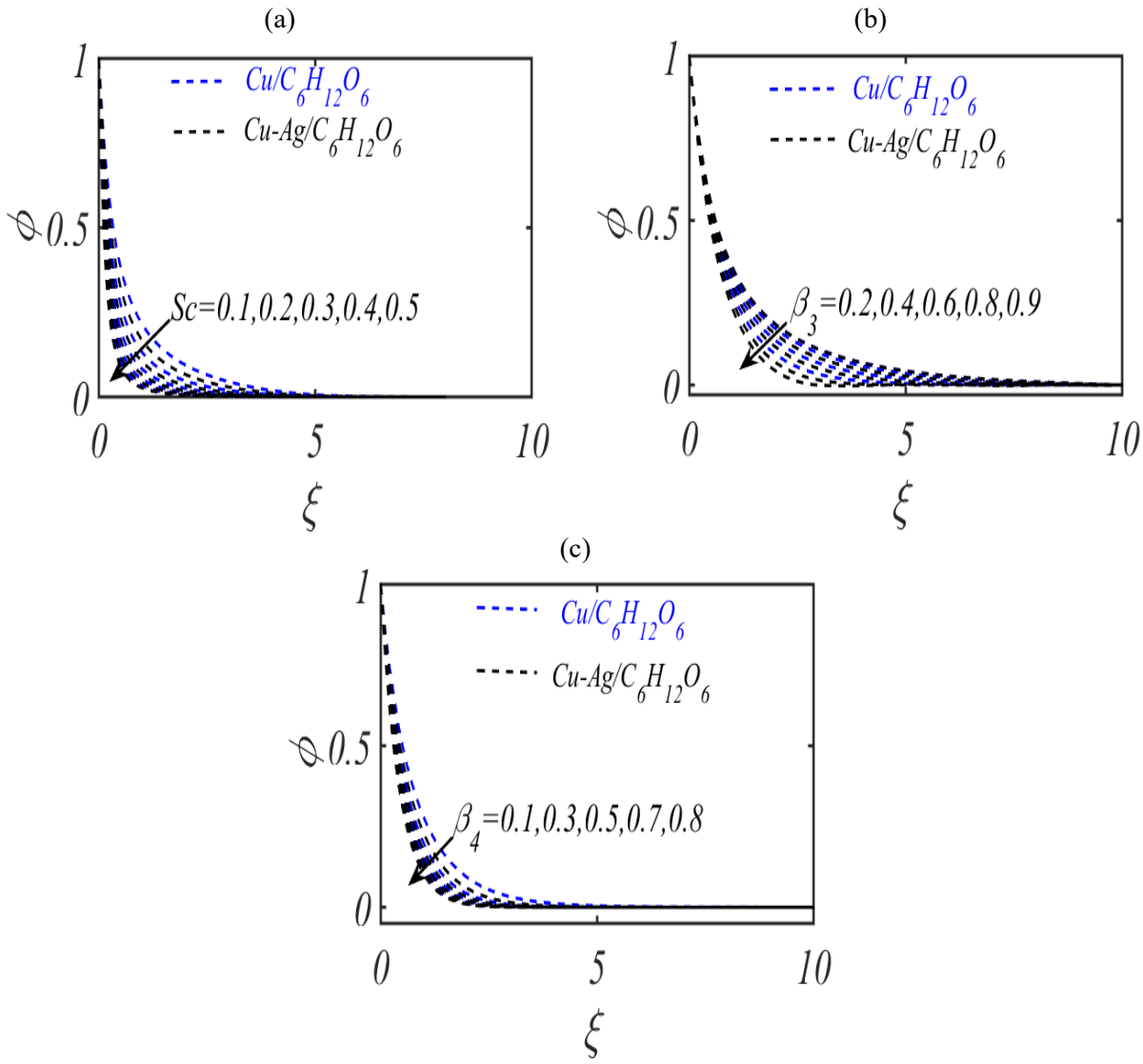

Figure. 4(a-c): Sophisticates the physical behavior of (a) Sc (b) β_3 (c) β_4 via Concentration profile ϕ.

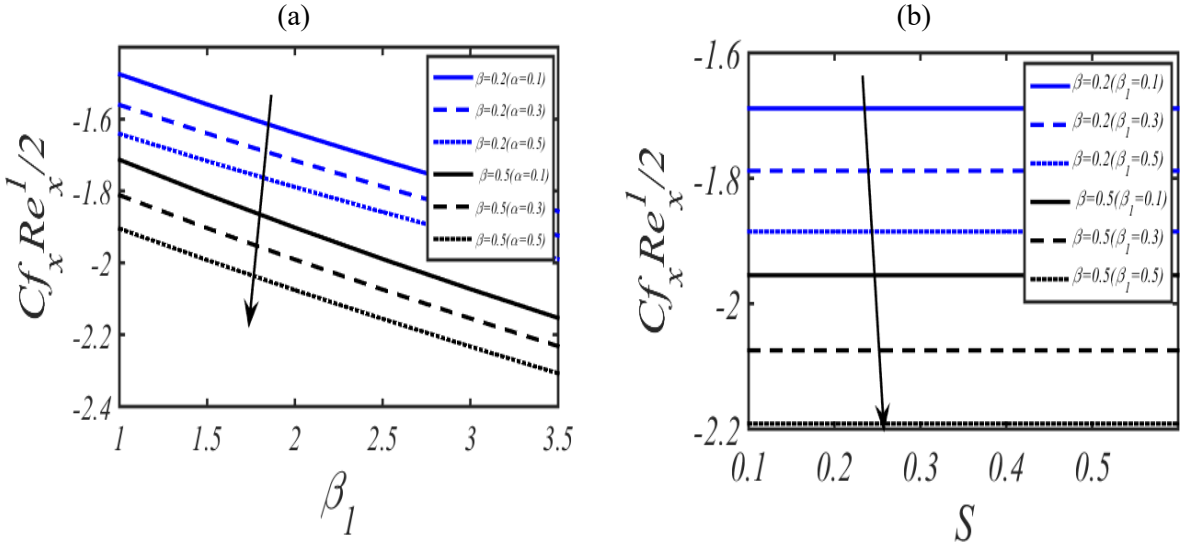

Fig. 5(a-b): exploits the variation of skin friction coefficient $Cf_x \operatorname{Re}_x^{1/2}$ (a) against β_1 for α (b) against S for β_1.

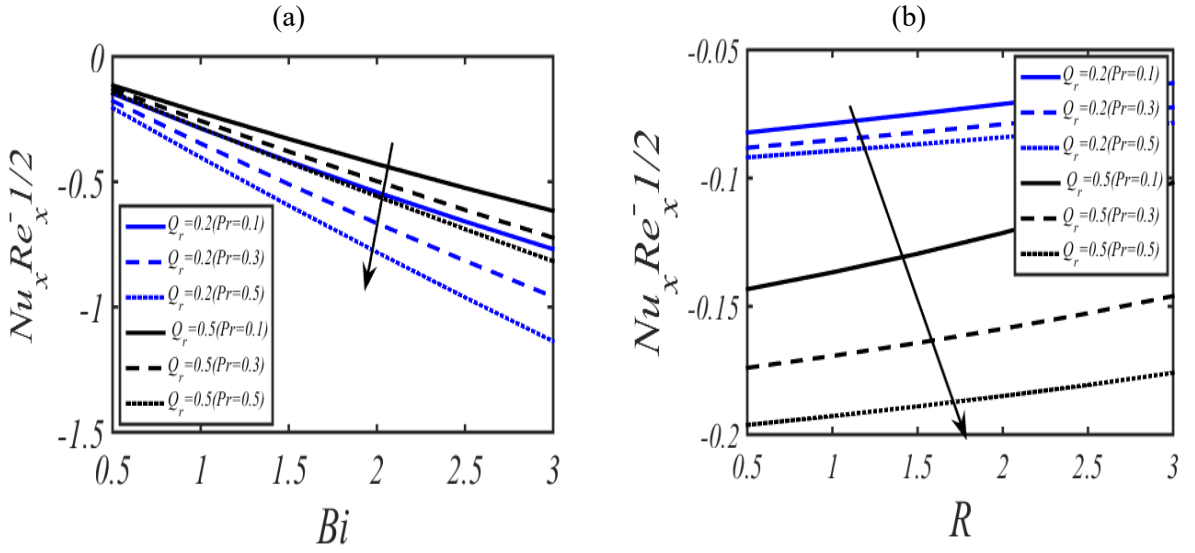

Fig. 6(a-b): exploits the variation of Nusselt number $\operatorname{Nu}_x \operatorname{Re}_x^{-1/2}$ (a) against Bi for Pr (b) against R for Pr.

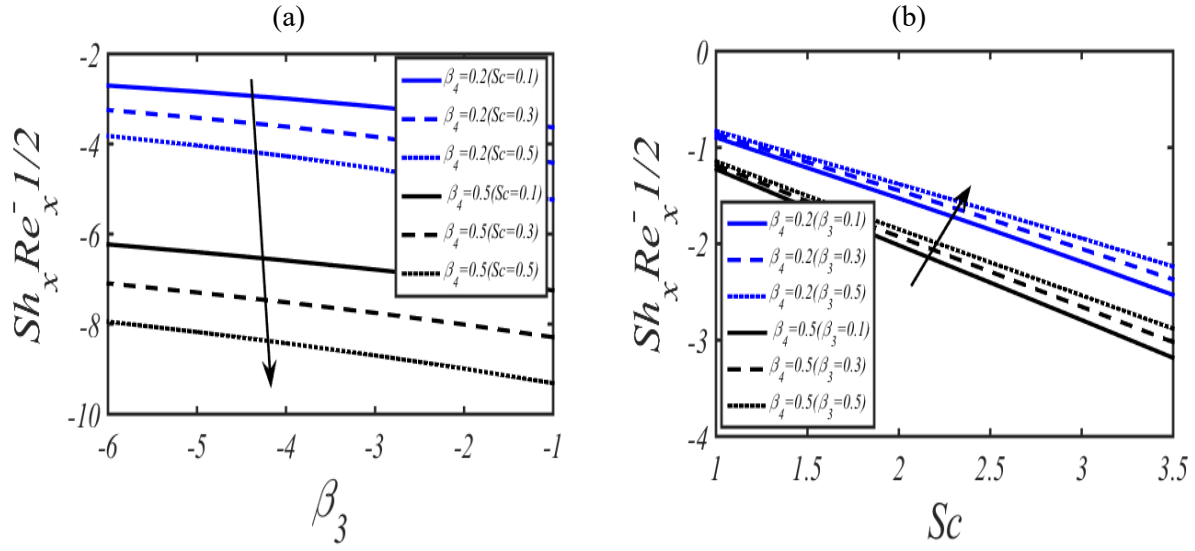

Fig. 7(a-b): exploits the variation of Sherwood number $Sh_x \operatorname{Re}_x^{-1/2}$ (a) against β_3 for Sc (b) against Sc for β_3.

Table 4: Variation of skin friction coefficient for various flow parameters.

α	β	β_1	$(Cu / C_6H_{12}O_6)$	$(Cu - Ag / C_6H_{12}O_6)$
0.5	0.5	0.2	1.3221230	1.5576939
1.5			0.639267	0.687225
1.8			0.470452	0.495649
	0.5		1.123950	1.124280
	0.8		0.704538	0.730633
	1.9		0.892510	0.905837
		0.5	1.871213	2.412077
		0.7	1.838027	2.355143
		0.9	1.803354	2.296493

Table 5: Influence of different fluid parameters on Nusselt number.

Ec	δ_T	R	Pr	θ_w	ϕ_1	$(Cu / C_6H_{12}O_6)$	$(Cu - Ag / C_6H_{12}O_6)$
0.2	0.1	0.3	0.7	0.5	0.3	2.124482	3.474889
0.4						2.168686	3.606232
0.6						2.208907	3.731419
0.3	0.2					0.550813	1.211454
	0.5					0.111072	0.263161
	0.8					0.010191	0.093086
		0.2				0.1535960	0.1711833
		0.6				0.1560604	0.1728267
		0.8				0.1573392	0.1738022
			0.2			0.1489145	0.1662272
			0.6			0.1573392	0.173802
			0.8			0.1426159	0.1828783
				0.4		0.2254604	0.2895505
				0.8		0.5903845	0.7615144
				1.2		0.6783576	0.8753674
					1.6	0.5408564	0.6719234
					2.5	0.7322893	0.9751963
					3.0	0.7565968	1.0355471

Table 6: Influence of different fluid parameters on Sherwood number.

Sc	β_3	β_4	$(Cu / C_6H_{12}O_6)$	$(Cu - Ag / C_6H_{12}O_6)$
2.5	0.5	0.2	0.140614	0.928862
3			3.546155	4.489948
3.5			4.209856	4.807153
	0.1		4.274518	4.554974
	0.2		4.275369	4.551655
	0.3		4.276220	4.548337
		0.6	1.279170	1.326730
		0.8	1.384949	1.456285
		0.9	1.479638	1.574516

6. Conclusions

- A reduction in the profile of velocity is examined for Hartmann number.
- The velocity profile increases due to Casson fluid parameter.
- The hybrid nanofluid shows a 15% enhancement compared with mono nanofluid.
- Enhancement of radiation parameter and coefficient of Biot number leads to improvement of heat transfer rate.
- Larger nanoparticles volume fraction results an improvement of thermal profile.
- The variation of Nusselt number against Biot number reduces when effects of Prandtl number are prominent.
- Variation of Casson fluid parameter on skin friction coefficient shows a declining trend.
- Current analysis can be further extended by incorporating the slip effects, bioconvection and machine learning simulations.
- The simulated results are based on theoretical assumptions under the ideal flow constraints, there may be discrepancies between the experimental data and theoretical results.

References

Acharya, N., et al. (2022). Hydrothermal variations of radiative nanofluid flow by the influence of nanoparticles diameter and nanolayer. *International Communications in Heat and Mass Transfer* 130, 105781.

Ahmed, F., et al. (2024). Numerical modeling of a MHD non-linear radiative Maxwell nano fluid with activation energy. *Heliyon* 10(2), e24098

Algehyne, E. A., et al. (2024). A numerical exploration of the comparative analysis on water and kerosene oil-based Cu–CuO/hybrid nanofluid flows over a convectively heated surface. *Scientific Reports* 14, no. 1 , 2540.

Ali, N., et al. (2021). Carbon-based nanofluids and their advances towards heat transfer applications—a review. *Nanomaterials* 11, no. 6,1628.

Alkasmoul, F. S., et al. (2025). Thermal performance and optimum concentration of different nanofluids in immersion cooling in data center servers. *Results in Engineering* 25, 103699.

Bani-Fwaz, M. Z., et al. (2024). Computational investigation of thermal process in radiated nanofluid modulation influenced by nanoparticles (Al2O3) and molecular (H2O) diameters. *Journal of Computational Design and Engineering* 11, no. 2, 22-36.

Bathmanaban, P., et al. (2024). Heat and mass transfer in double-diffusive mixed convection of Casson fluid: biomedical applications. *Colloid and Polymer Science* 302(10),1635-1669.

Bhatti, M. M., et al. (2023). The role of nanofluids in renewable energy engineering. *Nanomaterials* 13(19), 2671.

Dero, S., et al. (2022). Stability aspect of magnetized hybrid nanofluid with suction and injection phenomenon: Modified thermal model. *Journal of the Indian Chemical Society* 99, no. 9 ,100608.

Faridi, A. A., et al. (2025). Relaxation analysis and entropy simulation of triple diffusive slip effect on magnetically driven Casson fluid flow. *International Journal of Modelling and Simulation* 45, no. 5, 1753-1770.

Hayat, T., et al. (2023). Heat transfer and entropy analysis in squeezing flow of hybrid nanofluid (Au-CuO/NaAlg) with DF (Darcy-Forchheimer) and CC (Cattaneo-Christov) heat flux. *Materials Science and Engineering: B* 288,116150.

Hayat, T., et al. (2010). Heat and mass transfer for Soret and Dufour's effect on mixed convection boundary layer flow over a stretching vertical surface in a porous medium filled with a viscoelastic fluid, *Commun. Nonlinear Sci. Numer. Simul.* **15**, 1183–1196.

Iqbal, M. A., et al. (2025). Thermophoretic particle deposition in bioconvection flow of nanofluid with microorganisms and heat source: Applications of nanoparticle and thermal radiation. *Journal of Radiation Research and Applied Sciences* 18, no. 1, 101305.

Ishaq, M., et al. (2025). Thermal performance of casson hybrid nanofluid with radiative effects and convective conditions: applications to energy systems and industrial heat transfer. *Multiscale and Multidisciplinary Modeling, Experiments and Design*, *8*(2), 141.

Khan, K. A., et al. (2022). Analytical simulation of heat and mass transmission in casson fluid flow across a stretching surface. *Mathematical Problems in Engineering* 2022, no. 1, 5576194.

Khan, S. U., et al. (2025). Calorimetric and thermo-radiative analysis of hybrid nanofluid flow with chemical reactions using Cattaneo–Christov model. *Journal of Thermal Analysis and Calorimetry* 150, no. 18, 14649-14662.

Khoramian, R., et al. (2022). The development of novel nanofluid for enhanced oil recovery application. *Fuel* 311, 122558.

Kumar, T. S., (2021). Hybrid nanofluid slip flow and heat transfer over a stretching surface. *Partial Differential Equations in Applied Mathematics* 4, 100070.

Li, J., et al. (2021). Nanofluid research and applications: A review. *International Communications in Heat and Mass Transfer* 127, 105543.

Lone, S. A., et al. (2023). A stratified flow of a non-Newtonian Casson fluid comprising microorganisms on a stretching sheet with activation energy. *Scientific Reports* 13, no. 1, 11240.

Oudina, F., et al. (2024). Hybrid-nanofluid magneto-convective flow and porous media contribution to entropy generation. *International Journal of Numerical Methods for Heat & Fluid Flow* 34(2), 809-836.

Mishra, S., et al. (2023). Heat and mass transfer of water-based copper and alumina hybrid nanofluid over a stretching sheet. *Heat Transfer* 52(2), 1198-1214.

Moatimid, G. M., et al. (2024). Inspection of the nonlinear instability of electrified Casson fluids: a novel approach. *Waves in Random and Complex Media*, 1-31.

Muneeshwaran, M., G. et al. (2021). Role of hybrid-nanofluid in heat transfer enhancement–A review. *International Communications in Heat and Mass Transfer* 125, 105341.

Nabwey, Hossam A., et al. (2023). A comprehensive review of non-newtonian nanofluid heat transfer." *Symmetry* 15, no. 2 (2023): 362.

Pavía, M., et al. (2021), A critical review on thermal conductivity enhancement of graphene-based nanofluids." *Advances in Colloid and Interface Science* 294, 102452.

Rahman, M. A., et al. (2024). Review on nanofluids: preparation, properties, stability, and thermal performance augmentation in heat transfer applications. *ACS omega* 9(30), 32328-32349.

Sharma, Prabhakar, et al. (2022). Recent advances in machine learning research for nanofluid-based heat transfer in renewable energy system. *Energy & Fuels* 36(13), 6626-6658.

Sheikholeslami, M., et al. (2021). Recent progress on flat plate solar collectors and photovoltaic systems in the presence of nanofluid: a review. *Journal of Cleaner Production* 293,126119.

Wang, J., et al. (202). A review on nanofluid stability: preparation and application." *Renewable and Sustainable Energy Reviews* 188 (2023): 113854.

Waqas, H., et al. (2022). Heat transfer analysis of hybrid nanofluid flow with thermal radiation through a stretching sheet: A comparative study. *International Communications in Heat and Mass Transfer* 138, 106303.

Nomenclature

(u, v) Velocity components
ρ Density
h_f Heat transfer coefficient
R Thermal radiation parameter
C_f Coefficient of skin friction
Re_x Local Reynolds number
(ϕ_1, ϕ_2) Volume fraction
T_w Surface temperature
T Temperature
Bi Biot number
S Suction Parameter
B_0 Magnetic field strength
k Thermal conductivity
C_p Specific heat capacity
q_r Radiative heat flux
a Stretching ratio parameter
β Casson fluid parameter
β_1 Hartmann parameter
(x, y) Coordinates
T_∞ Ambient temperature
γ Temperature gradient
θ_w Temperature Ratio Parameter
Sh_x Sherwood number
β_3 Thermal concentration number
Ec Eckert number
β_4 Chemical reactive parameter
Pr Prandtl number
δ_T Thermal relaxation number
f' Velocity profile
θ Temperature profile
ϕ Concentration profile